PAPER

Structure and anomalous underscreening in ethylammonium nitrate solutions confined between two mica surfaces†

Y. K. Catherine Fung [ID] and Susan Perkin [ID]*

The observation of long-range interactions across ionic liquids and highly concentrated electrolytes, extending far beyond the Debye–Hückel prediction and beyond the range predicted in liquid state theory, has been called 'anomalous underscreening'. A number of theoretical and experimental works have explored this phenomenon over recent years, although its origin is not yet fully understood. Most of the experimental studies of anomalous underscreening until now involved aprotic ionic liquids, and so it is of interest to explore interactions in protic ionic liquids where the distribution of charge in the fluid is different in nature. Here we present direct measurements of the interaction force as a function of separation distance, measured using a surface force balance, across solutions of a protic ionic liquid ethylammonium nitrate (EAN) and its mixtures with water over a range of volume fractions from 10 vol% to 100 vol% EAN. The results reveal intricate details about near-surface ordering and dynamics at the EAN–mica interface as well as anomalous underscreening consistent with that observed in the past with aprotic ionic liquids.

I.   Introduction

Electrolytes at high concentration are important in fields as diverse as energy storage, bioscience, and mineralogy. They provide the medium for charge transfer, for mediating macromolecular interactions, and for the nucleation of crystals. Despite this general relevance, some fundamental aspects of the physics and physical chemistry of highly concentrated electrolytes remain mysterious. In particular, several experimental reports have indicated interaction forces acting over substantially longer range than previously anticipated in ionic liquids and concentrated electrolytes. The first of these reports, now more than a decade ago, measured interactions between two macroscopic charged plates over a range of tens of nanometers across a pure ionic liquid at ambient temperature; a range

Physical & Theoretical Chemistry Laboratory, University of Oxford, Oxford, UK. E-mail: susan.perkin@chem.ox.ac.uk
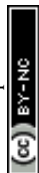
enormously greater than the relevant Debye screening length.[1] Since then similar phenomena have been reported, mostly involving interaction force measurements with a surface force balance (SFB)[2–5] or AFM[6] but also concentration profile measurements between two silica surfaces.[7]

The general form of the measured interaction force, and corresponding free energy, across concentrated electrolytes in these experiments was captured approximately by the following expression:

$$\frac{F_N}{R} = 2\pi G^{\parallel} = -\frac{H}{6D^2} + Ae^{-D/\lambda_o}\cos\left(\frac{2\pi D}{\xi} + \phi\right) + Be^{-D/\lambda_s} \qquad (1)$$

where F_N is the force measured between crossed cylinders of radius R and closest separation distance D, which is related to the free energy per unit area between flat plates, $G^{\parallel}$ at separation D through the Derjaguin approximation.[8] F_N, R and D are obtained from experimental measurement directly. H is the Hamaker constant calculated from Lifshitz theory. The first term on the right of eqn (1) represents the van der Waals interaction and tends to be small compared to the other terms at high electrolyte concentrations and high surface charge. The second term on the right has been described as the 'structural force' arising from steric effects of ions and molecules packed into the confined region. The final term, a plain exponential, describes the resultant 'electrostatic force'. The parameters for the 'structural' and 'electrostatic' terms, A, λ_o, ξ, ϕ, B and λ_s can be fitted to the experimental data but are also defined in theories of electrolytes and so provide a link for interpretation of measurements using theoretical analysis.

In dilute electrolyte solutions the same expression, eqn (1), explains experimental interaction forces and is well understood theoretically.[9] In that case the van der Waals and electrostatic terms together make up the mean-field DLVO theory[10] with λ_s then matching the Debye–Hückel screening length, λ_D, where:

$$\lambda_D^{-2} = \kappa_D^{2} = \frac{\sum_i n_i^b q_i^{2}}{\varepsilon_r \epsilon_0 k_B T} \qquad (2)$$

with n_i^b the bulk salt concentration, q_i is the charge on ion i, ε_r the dielectric constant of the medium, ϵ_0 the vacuum permittivity, k_B is Boltzmann's constant and T the temperature. The second, oscillatory, term matches the (non-mean field) structure of the molecular solvent (e.g. water structure) as can be resolved in the highest resolution measurements in dilute electrolytes.[9,11]

Why should such an expression also model the observed behaviour in a concentrated electrolyte, so far from the regime where mean-field theories apply? An answer may lie in the exact analysis of the decay of intermolecular correlations in electrolytes by Kjellander.[2,12] Taking account of all ion correlations and with proper analysis of the dielectric response, Kjellander showed that the decay of interaction free energy with distance has multiple terms, each either plain exponential or exponentially damped oscillatory. The decay parameter for each term (or 'mode') is a solution of the following equation:

$$\lambda^{-2} = \kappa^{2} = \frac{\sum_i n_i^b q_i^* q_i}{\varepsilon_r^*(\kappa)\epsilon_0 k_B T} \qquad (3)$$

where q_i^* is the renormalised charge and $\varepsilon_r^*(\kappa)$ is the renormalised dielectric function (a function of κ, so that eqn (3) is an equation for κ). Thus, interactions
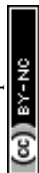
are characterised by multiple decay parameters and in general each parameter reflects both charge and density correlations; *i.e.* there is no single 'electrostatic decay length'.[12] In the limit of infinite dilution, the slowest decaying term is plain exponential, and the decay length collapses onto the Debye–Hückel screening length. At a high concentration of electrolyte, the presence of a slowly decaying plain exponential term must arise from a small value of q_i^*. (Note that the dielectric function is approximately the dielectric constant when the decay parameter is small.) This has been interpreted in the past in terms of strongly coupled ion aggregates behaving as quasiparticles,[2] and as voids in the ionic network performing the role of charge carrier over length scales characterised by the Bjerrum length.[13] However, it remains challenging to calculate values for q_i^* and $\varepsilon_r^*(\kappa)$ and so the connection to experiments is yet to be fully clarified.

A particular feature of the experimental measurements in concentrated electrolytes is that the range of electrostatic interactions, characterised by λ_s in eqn (1), was found to increase with increasing ion-concentration of the electrolyte[3] and appeared to follow a scaling relation as follows:[14]

$$\left(\frac{\lambda_s}{\lambda_D}\right) \sim \left(\frac{a}{\lambda_D}\right)^v \tag{4}$$

With the exponent $v \approx 3$ across a range of experimental conditions. This phenomenon, in which charged bodies or surfaces interact in a manner that appears less screened than predicted by mean field theories, has been called 'underscreening',[14] or 'anomalous underscreening'.[15]

However, substantial effort to reproduce and interpret the decay of interactions using theory and computer simulations have not yet matched up with the experiments: the increase of screening length with concentration was apparent, but the scaling was very different to experimental values (giving $v \approx 2$) and the decay of correlations was oscillatory rather than plain exponential.[16–21] Only one recent analysis of the restricted primitive model electrolyte has shown the longer-ranged monotonically decaying term similar to experimental observations.[22] Furthermore, in some recent measurements of forces across concentrated aqueous electrolytes with AFM no long range forces were apparent;[15] the full picture remains to be fully revealed. The significance and implications of interactions across electrolytes, for a multitude of applications and for our understanding of electrostatics in the liquid state, motivate us to investigate more deeply the phenomena involved.

Here, we study the interaction forces between mica sheets across ethylammonium nitrate (EAN) and its mixtures with water. In contrast to the majority of electrolytes used in the experiments mentioned above, EAN is a protic ionic liquid. Previous experiments involved aprotic ionic liquids, either pure or mixed with polar solvent, or inorganic salts in water. Mindful of the importance of charge distribution in the fluid, it will be of interest to investigate the similarity or otherwise of interactions across aprotic and protic salts. In protic fluids charge transfer can follow a hopping mechanism, known as the Grotthuss mechanism, which accounts for the high conductivity of acidic aqueous solutions compared to salt solutions at similar charge density. Furthermore, the quantum nature of hydrogen bonds and the distribution of charge in protic fluids is of current interest.[23,24]

Even though there have been relatively few studies of interactions in protic ionic liquids, in fact the first surface force measurements across an ionic liquid involved EAN and its mixtures with water.[25] In those experiments the oscillatory structural forces were evident and the changing features with concentration were carefully analysed. However, the less-fine resolution available at the time of those measurements precluded any measurement of weak longer-ranged forces (beyond the oscillatory structural force) as have subsequently been seen in non-protic ionic liquids. Subsequent studies of EAN on mica surfaces were made by Atkin and Warr,[26] where again the alternating repulsive and attractive forces indicated layering at the interface. The observed wavelength of 0.5 nm is comparable to the EAN ion-pair size. Small-angle neutron scattering experiments of EAN at $T = 318$ K (ref. 27) revealed nanostructure in the bulk fluid, likely arising from aggregation of the non-polar groups and of the charged groups in sponge or smectic phases. The addition of water, creating EAN aqueous mixtures, was found to have dramatic effects on surface forces and particle stability.[28] Silica colloids were found to be stable in pure EAN, understood through direct AFM force measurement to be due to the build-up of strong solvation layers at the silica interface. However, addition of water led to weaker solvation and fewer solvation layers, and at 5 wt% EAN in water the interaction force between silica surfaces contained an attractive region which led to instability of silica colloids in the mixture. The bulk structure of the EAN–water mixtures has been studied using X-ray scattering, revealing nanostructure consisting of bicontinuous ionic and aqueous phases with local structure remarkably similar to the pure fluids.[29]

In the measurements presented here we resolve the interaction forces in EAN and water mixtures at higher resolution and over longer range, and compare the results to literature measurements of non-protic electrolytes. Our measurements confirm that the functional form expressed in eqn (1) is a suitable framework for describing forces across EAN solutions, and we describe and interpret the parameters.

The damped oscillatory term appears to describe structural forces (density correlations), with wavelengths comparable to the ion-pair size, in highly concentrated solutions (>80 vol% EAN). At lower concentrations, oscillations are not resolved. Interestingly, in some cases, we found that the nature of the oscillatory force is dependent on the timescale of compression and measurement, indicating slow dynamical effects in the confined structured fluid. At high concentrations we also observe a longer-range plain exponential 'tail' in the force, with exponential decay length consistent with previous measurements in non-protic ionic liquids and simple inorganic salt solutions. The concentration-dependence also mirrors earlier measurements, in that the range of the force increases with increasing EAN salt concentration.

II. Methods

Surface forces measurements between two atomically smoothed mica surfaces across ethylammonium nitrate (EAN) were carried out with a Surface Forces Balance (SFB) using methods described in detail recently.[9,30] Briefly, the SFB utilises white light interferometry to measure surface separation and determine the deflection of a spring, from which the force as a function of the surface separation can be obtained. Muscovite mica (V-1 optical grade, S&J Trading) was
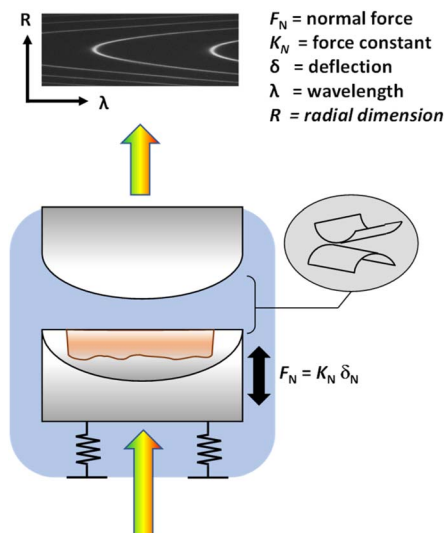
Fig. 1 Schematic diagram of the Surface Force Balance (SFB). Collimated white light passes through two cylindrical lenses in crossed-cylinder orientation. Back silvered mica sheets which allow light to reflect and partially transmit are glued onto the lenses as a surface substrate. The transmitted light enters a spectrometer and produces interference patterns of fringes of equal chromatic order (FECO). Surface separation, D, is obtained by analysing the FECO.[31]

cleaved to <7 μm in thickness. Approximately 45 nm silver was deposited to the back of the mica sheet using vapour deposition. The back silvered mica sheets were fixed onto two cylindrical lenses using an epoxy glue (EPON 1004, Shell Chemicals). One lens was mounted onto a leaf spring in a stainless-steel boat while the other lens onto a piezoelectric tube. Bright white light is shone vertically through the silver–mica–film–mica–silver cavity, and the resulting fringes of equal chromatic order (FECO) are used to determine the mica thickness and surface separation with high resolution (Fig. 1).

Our setup affords a very high precision in distance of 0.1 nm; accuracy is about 0.2 nm within a single experiment or about 0.5 nm between separate experiments. Furthermore, our resolution in force is $\sim 10^{-7}$ N, between atomically smooth mica crystals of curvature radius $R \approx 10^{-2}$ m, giving resolution in $G^{\parallel} \sim \dfrac{F_N}{R} \approx 10^{-5}$ J m^{-2}. (This compares favourably with AFM where resolution in force is $\sim 10^{-12}$ N but the roughness of AFM probes tends to lead to actual asperity curvature of $R \approx 10^{-8}$–10^{-9} m, so $G^{\parallel} \sim \dfrac{F_N}{R} \approx 10^{-3} - 10^{-4}$ J m^{-2} for AFM.)

Equimolar nitric acid and ethylamine were reacted in an ice bath to produce ethylammonium nitrate (EAN). The water was removed with a rotatory evaporator at 40 °C until there was no further visible change of the liquid level. The product was then placed on a Schlenk line over 72 h at 30 °C to remove any excess water. The water content of neat EAN measured with the Karl Fischer titrator (HI934, Hanna Instrument) was below 0.1 wt%. Refractive index measurements using an Abbe 60 refractometer gave a value of 1.45, 1.44, 1.43, 1.42 and 1.35 for 100%, 90 vol%, 80 vol%, 70 vol% and 10 vol% EAN respectively.
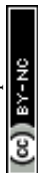
Table 1 Summary of fitted decay lengths and oscillatory wavelengths for different volume fractions of EAN at high concentrations

EAN volume fraction	λ_s	λ_o	ξ
1	7.6 ± 1.4	1.3 ± 0.2	0.5 ± 0.2
0.9	7.3 ± 1.5	1.1 ± 0.1	0.5 ± 0.2
0.8	7.1 ± 1.1	1.7 ± 0.2	0.6 ± 0.2

III.   Measured interaction forces across ethylammonium nitrate solutions

We performed force measurements with 100 vol% (11.2 M), 90 vol% (9.9 M), 80 vol% (8.7 M), 70 vol% (7.9 M) and 10 vol% (1.1 M) EAN. Fig. 2, 3 and 4 show example force measurements of 100 vol%, 90 vol% and 80 vol% EAN respectively. In all three concentrations, we show both approach and retraction in (a), and a fit to eqn (1). As indicated before, λ_s, λ_o, and ξ are fitting parameters. These can be obtained from the experimental data shown in (b), (c) and (d) respectively in the corresponding figure. These parameters at each concentration are summarised in Table 1.

A.   Neat EAN (100 vol%)

Fig. 2 shows example measurements between two mica sheets across 100 vol% EAN. In (a) and (b) we show the normalised forces on linear and semi-logarithmic scales. In the range of mica separations 2 nm < D < 5 nm, the interaction force oscillates between positive and negative values, as most clear on the linear scale where force minima are also presented. Our experimentally accessible range of applied force prevented study of the range below $D = 2$ nm. From the variation of the force minima with distance (Fig. 2(c)) we obtain the parameter $\lambda_o = 1.3 \pm 0.2$ nm, and from the separation distance between minima (Fig. 2(d)) we obtain the oscillatory wavelength, $\xi = 0.5 \pm 0.2$ nm. This measured wavelength is comparable to the wavelengths measured for structural forces in neat EAN by Horn[25] and by Atkin.[26] This value also corresponds closely with the characteristic size of an EAN ion pair calculated by taking the cube root of the ion-pair volume, which in turn is from the bulk fluid density, ~ 0.53 nm.

Beyond $D = 5$ nm, we observe a non-oscillating force which decays with increasing distance in an apparently exponential form, Fig. 2(b). The mean average decay parameter for this longer-ranged force in 100 vol% EAN is found to be $\langle \lambda_s \rangle = 7.6 \pm 1.4$ nm (from 3 separate experiments, each with different mica sheets and EAN samples; see ESI†).

The reported long-range decay here, measured at room temperature, is comparable to the decay length of 6.3 nm reported in the AFM measurement by Hjalmarsson and co-workers between mica and silica at 373 K and 393 K.[6] The surface charge of silica has been reported to increase at elevated temperature in water,[32] perhaps explaining the appearance of this additional interaction between silica and mica surfaces above a threshold temperature in the AFM measurements with EAN.
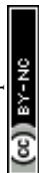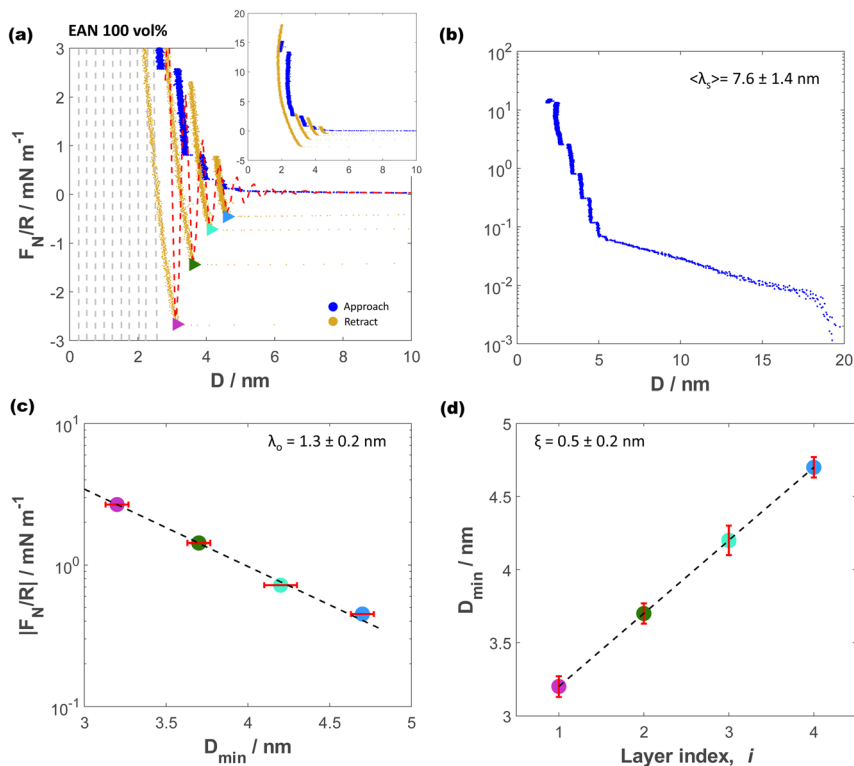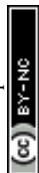
Fig. 2 Example measurements of the normalised force between mica sheets as a function of separation, D, across 100 vol% EAN. (a) Linear scale forces at $D < 10$ nm with retraction (gold) shown from each layer. Red dashed line shows the force fitted using eqn (1) and the parameters reported in Table 1. Inset shows the full magnitude of the force. (b) Log–linear representation of normal force displaying long-range decay with average decay length $\langle \lambda_s \rangle = 7.6 \pm 1.4$ nm. (c) The exponential decay envelope is calculated from the force minima, giving $\lambda_o = 1.3 \pm 0.2$ nm. (d) The distance separation between the minima gives the oscillation wavelength of the structural force, here $\xi = 0.5 \pm 0.2$ nm.

B. 90 vol% EAN

Fig. 3 shows example measurements between two mica sheets across 90 vol% EAN mixture with water. The interaction force is presented on linear and semi-logarithmic scales in panels (a) and (b). As for the neat EAN, we find oscillations between repulsive and attractive forces, this time in the range 1 nm $< D <$ 5 nm. By fitting the oscillations (Fig. 3(c)) we obtain $\lambda_o = 1.1 \pm 0.1$ nm, and from the separation distance between minima (Fig. 3(d)) we obtain the oscillatory wavelength, $\xi = 0.5 \pm 0.2$ nm. There is little impact of introducing 10 vol% of water into the EAN; very slight differences are the reduction in the number and definition of the layers. Now 6 distinct layers are observable on surface approach compared to 7 layers in neat EAN. In addition, the 5th and the 6th layer are less defined compared to that of neat EAN. Again in 90 vol% EAN, similar to the 100 vol% EAN experiments, we observe a plain exponential tail in the force at larger distances with $\langle \lambda_s \rangle = 7.3 \pm 1.5$ nm.
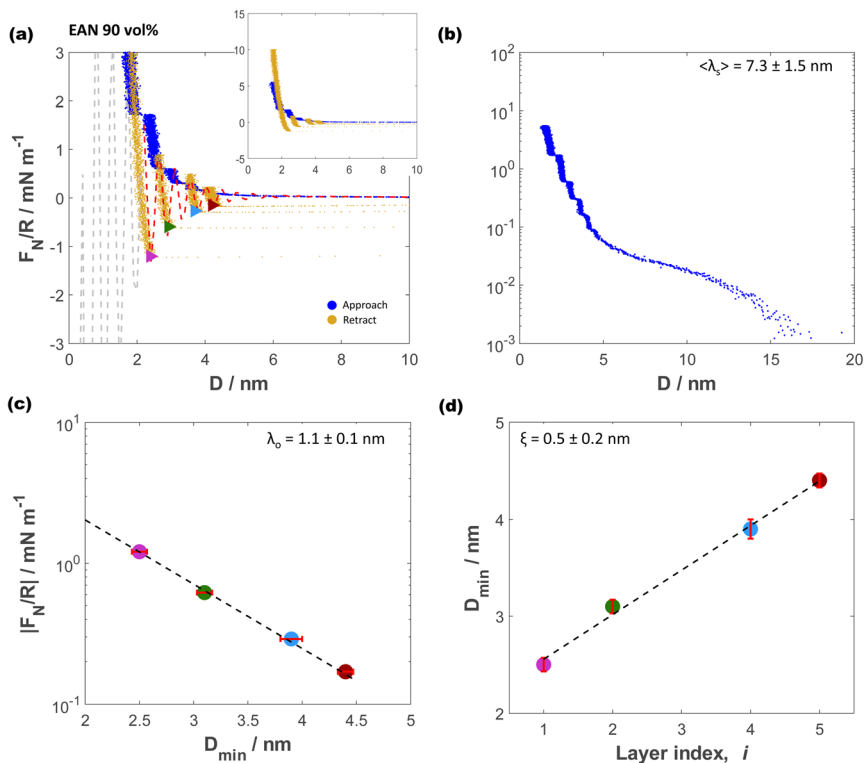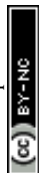
Fig. 3 Example measurements of the normalised force between mica sheets as a function of separation, D, across 90 vol% EAN. (a) Linear scale forces at $D < 10$ nm with retraction (gold) shown from each layer. Red dashed line shows the force fitted using eqn (1) and the parameters reported in Table 1. Inset shows the full magnitude of the force. (b) Log–linear representation of normal force displaying long-range decay with average decay length $\langle \lambda_s \rangle = 7.3 \pm 1.5$ nm. (c) The exponential decay envelope is calculated from the force minima, giving $\lambda_o = 1.1 \pm 0.1$ nm. (d) The distance separation between the minima gives the oscillation wavelength of the structural force, here $\xi = 0.5 \pm 0.2$ nm.

C. 80 vol% EAN

Fig. 4 shows example measurements between two mica sheets across the mixture of 80 vol% EAN and 20 vol% water. The interaction force is presented on linear and semi-logarithmic scales in panels (a) and (b). The oscillatory force, again below $D \sim 5$ nm, is qualitatively similar to those seen in the more concentrated electrolytes. However the details are slightly modified by the increased fraction of water: as shown in Fig. 4(a) (linear–linear) and Fig. 4b (log–linear), there are now only 4 distinct layers observed on approach. The oscillatory wavelength is similar to the EAN ion-pair dimension, $\xi = 0.6 \pm 0.2$ nm, however the oscillatory forces have a slightly longer decaying envelope with $\lambda_o = 1.7 \pm 0.2$ nm. Beyond $D = 5$ nm there remains a longer ranged force, decaying apparently exponentially with distance up to ~ 15 nm, with an average screening length of $\langle \lambda_s \rangle = 7.1 \pm 1.1$ nm.
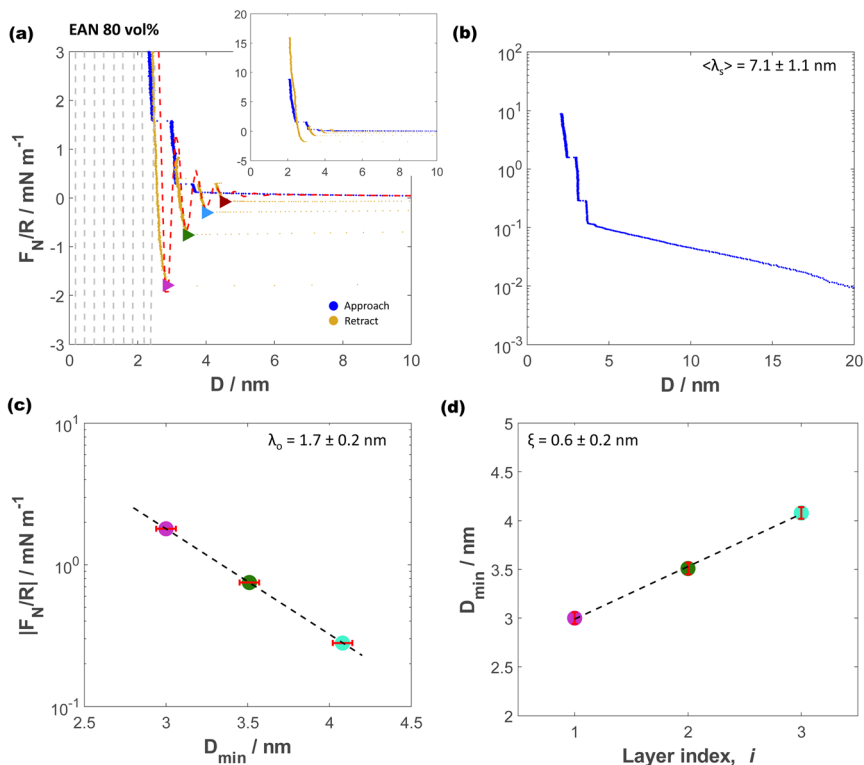
Fig. 4 Example measurements of the normalised force between mica sheets as a function of separation, D, across 80 vol% EAN. (a) Linear scale forces at $D < 10$ nm with retraction (gold) shown from each layer. Red dashed line shows the force fitted using eqn (1) and the parameters reported in Table 1. Inset shows the full magnitude of the force. (b) Log–linear representation of normal force displaying long-range decay with average decay length $\langle \lambda_s \rangle = 7.1 \pm 1.1$ nm. (c) The exponential decay envelope is calculated from the force minima, giving $\lambda_o = 1.7 \pm 0.2$ nm. (d) The distance separation between the minima gives the oscillation wavelength of the structural force, here $\xi = 0.6 \pm 0.2$ nm.

D. 70 vol% EAN

When the water content was increased to 30 vol%, with 70 vol% EAN, the effect on near interface structure and on the long-range decay is substantial: forces are presented in Fig. 5 on linear scales in (a) and semi-logarithmic scales in (b). As shown in Fig. 5(a), the definition of the layers is much reduced: a small kink in the approach curve is discernible, but there are no clearly resolved oscillatory forces. Nonetheless, there is a hysteresis observed on retraction indicating an energy minimum. Beyond $D = 5$ nm there remains a longer ranged force, decaying apparently exponentially with distance up to ca. 15 nm, with an average screening length of $\langle \lambda_s \rangle = 3.8 \pm 1.2$ nm.

E. 10 vol% EAN

We have performed two experiments at a more dilute regime of 10 vol% EAN water, and observed different behaviour in the two experiments and thus
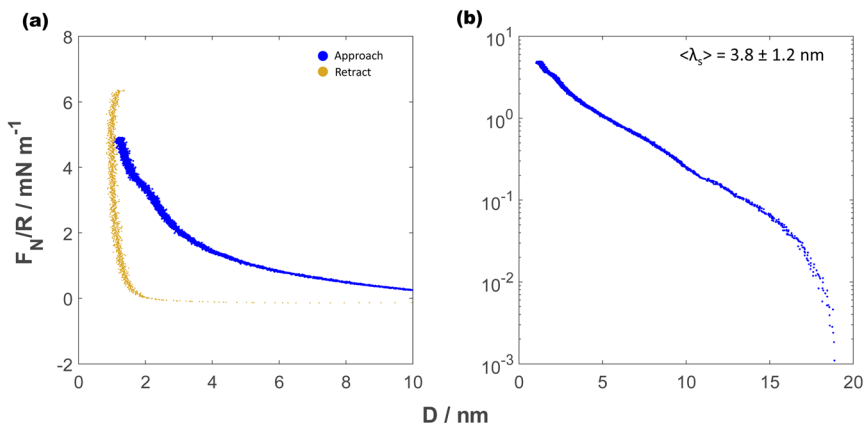
Fig. 5 Measurements of the normalised force between mica sheets as a function of separation, D, across 70 vol% EAN. (a) Linear scale forces at $D < 10$ nm with retraction (gold) shown from the innermost layer. (b) Log–linear representation of normal force displaying long-range decay with average decay length of $\langle \lambda_s \rangle = 3.8 \pm 1.2$ nm.

example force profiles from each of the two experiments are presented in Fig. 6. In the first set of measurements, shown in Fig. 6(a) and (b), there was a soft repulsive force (no oscillations) at short range and a very short exponential tail with decay length of about $\lambda_s = 0.8$ nm. However, in the second set of measurements, in Fig. 6(c) and (d), there was a small attractive force from about 4 nm and no measurable exponentially decaying repulsion beyond this. To interrogate the origin of the difference between these experiments, we note that very tiny changes to the concentration of EAN are known to give rise to very different behaviours around this volume fraction. In Horn's experiments,[25] repulsive forces were measured at concentrations both below and above 10 vol% EAN, but attractive forces were measured (only) around 10% EAN. It appears that this concentration represents a tipping point between two driving forces for repulsion: classical 'double layer' forces in more dilute solutions, and 'under-screening' at higher concentrations. It may be that small variation in the actual EAN volume fractions in our two experiments have led to probing of two distinct behaviours.

IV. Variation of λ_s with concentration

We now consider and interpret the plain exponential decay length, λ_s, of the long-range part of the forces observed in the present measurements with EAN–water mixtures. Past measurements of interactions across concentrated electrolytes, revealing similar asymptotic plain exponential decay and interpreted with eqn (1), suggested a scaling of the screening length as outlined in eqn (4). Within the same framework, we plot our measured λ_s values for each concentration in terms of the dimensionless λ_s/λ_D *vs.* a/λ_D in Fig. 7. Noting that the Debye length, λ_D, varies with concentration and dielectric constant according to eqn (2), the parameter a/λ_D increases according to $(n_i^b/\varepsilon_r)^{1/2}$ for any fixed salt (*i.e.* fixed value of a) and temperature. In order to carry out this analysis we have
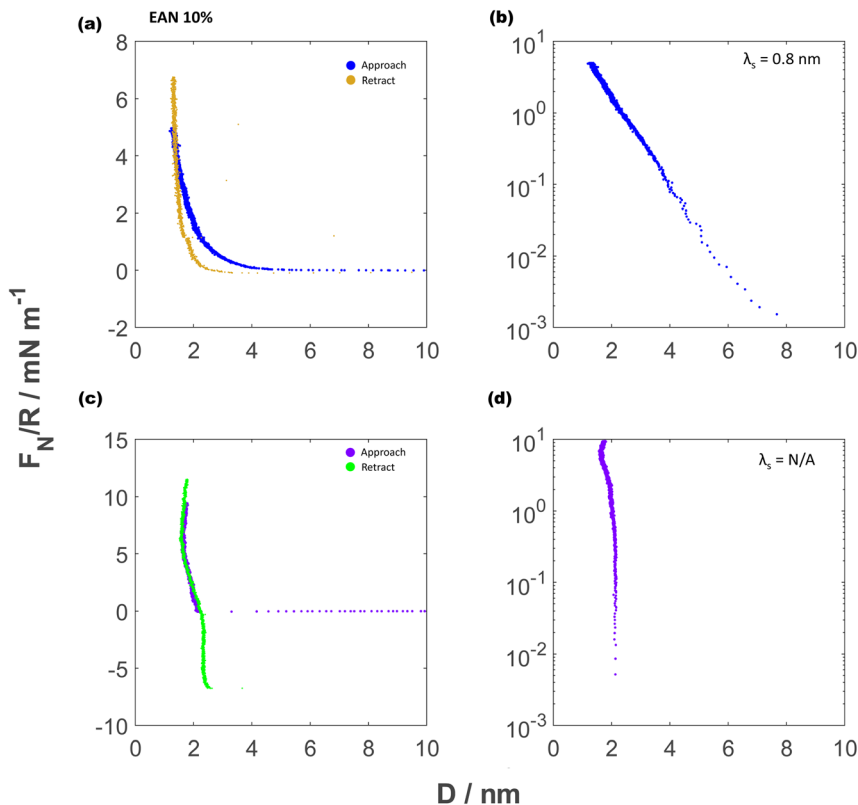
Faraday Discussions

Fig. 6 Measurements of the normalised force between mica sheets as a function of separation, D, across 10 vol% EAN. (a) and (b) are data from experiment #1 and (c) and (d) are data from experiment #2. (a) Linear scale close up at $D < 10$ nm with retraction (gold) showing at the innermost layer. (b) Log–linear representation of normal force displaying long-range decay with decay length of $\lambda_s = 0.8$ nm. (c) Linear scale close up at $D < 10$ nm with retraction (green) showing at the innermost layer. (d) Log–linear representation of normal force showing no decay length.

calculated the bulk dielectric constant from effective medium theory for each EAN–water mixture (see ESI Table 1†). The mean ion diameter, a, does not vary with concentration and is calculated as $a = \sqrt[3]{\dfrac{v_m}{2}}$, where v_m is the ion pair volume calculated from the bulk density and molecular mass. With this analysis, we observe that our measured screening lengths, when normalised by the respective Debye lengths, vary with concentration in a systematic way and correspond reasonably closely to previously reported measurements with a range of different (non-protic) concentrated electrolytes. In general, our results contribute evidence in support of the former observations regarding scaling of the screening length; at least for the case of measurements made between mica sheets using the surface force balance. It appears that the protic nature of the EAN solutions studied here does not give rise to any substantial deviation from the former observation.
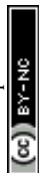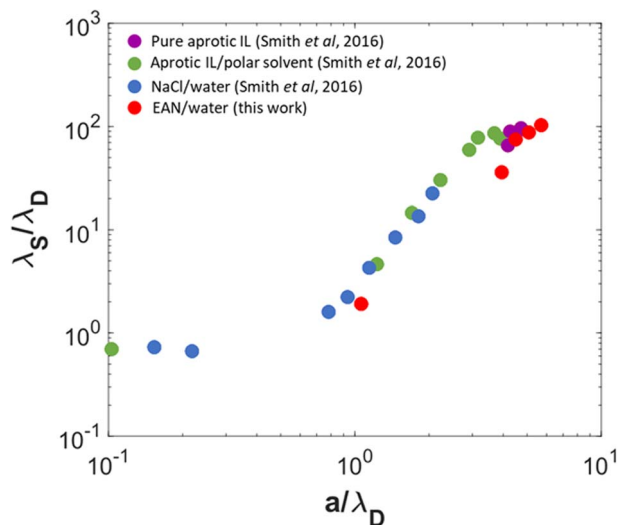
Fig. 7 Experimental decay length normalised by the corresponding Debye length, λ_s/λ_D, as a function of the mean ion diameter normalised by the Debye length, a/λ_D. Data points are show for literature measurements by Smith et al.[3] and, in red, the measurements with EAN reported in this work.

V. Dynamic features of the short-range forces

During our experiments reported above for EAN–water mixtures at volume fractions between 80 vol% EAN and 90 vol% EAN we noticed some interesting dynamic features regarding the short-range oscillatory forces, indicating variation
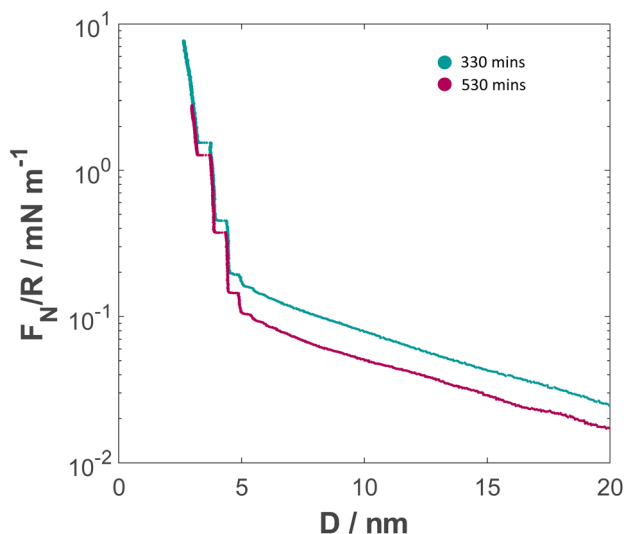

Fig. 8 Time evolution of the normalised force between mica sheets as a function of separation, D, across 100% EAN.

Faraday Discussions

in the near-surface structure and dynamics. Here, we outline some of these observations and consider their likely origin.

For contrast, we begin by showing that the interaction forces across 100 vol% EAN do not appear to vary significantly over time (see Fig. 8). As already outlined above, in neat EAN we observed distinct layers near the mica–EAN–mica interface during surface approach. These layers are well defined during our slow approach (approach rate 0.42 ± 0.09 nm s^{-1}). Fig. 8 shows two force profiles recorded from two different approaches across 100 vol% EAN between mica sheets at different times after injection of EAN between the mica sheets; apart from a small vertical offset which is likely due to different mica charge, the two force profiles are very similar.

However, when we perform force measurements with 90 vol% and 80 vol%, we observed dynamic features. In Fig. 9, we show that despite using a slow approach rate of 0.42 ± 0.16 nm s^{-1}, towards the beginning of the measurement (Fig. 9(a)) the
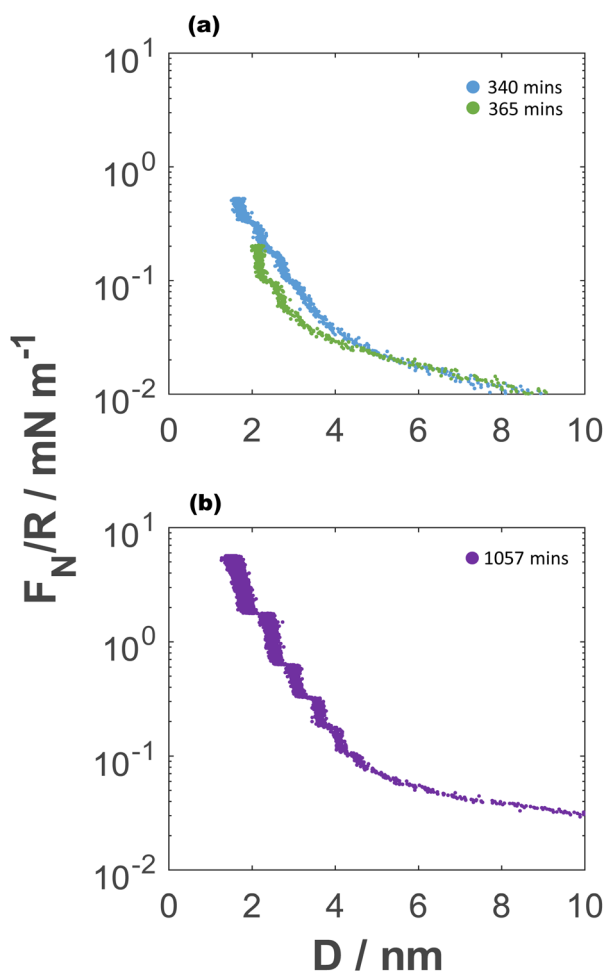

Fig. 9 Time evolution of the normalised force between mica sheets as a function of separation, D, across 90 vol% EAN at the same spot. (a) Measured at 340 min and 365 min after liquid injection. (b) Measured at 1057 min after liquid injection.
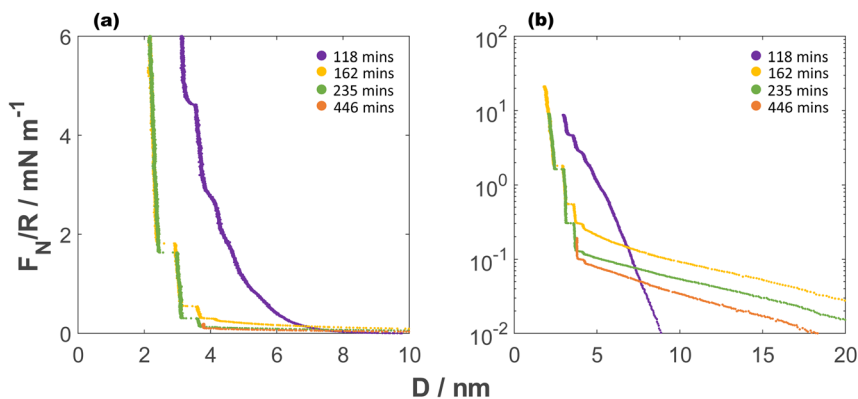
Fig. 10 Normalised force profiles as a function of surface separation for 80 vol% EAN. (a) Surface separation less than 10 nm showing 4 different profiles measured at different time after liquid injection: purple at 118 min, yellow at 162 min, green at 235 min and orange at 446 min. (b) Log–linear scale of the same profiles as (a) with surface separation displayed up to 20 nm.

layers are visible but not well defined. After longer times within the same experiment, Fig. 9(b), we observed the layers to become more well defined. 90 vol% EAN has a viscosity of about 8 mPa s (ref. 33) which is approximately 5 times less viscous than neat EAN; at this approach rate we do not see any variation in the longer range forces with varying velocity, and so the measurement is considered to be 'quasi-static'. Thus, the variation in the near-surface forces with measurement time on the order of several hours appears to indicate a changing nature of the interfacial structure over this timescale. It is also possible that very small variations in the water content may occur over such times, although the observation of further variations over time at different water fractions indicates a different mechanism.

For 80 vol% EAN (Fig. 10), we observed less-defined layers as well as different asymptotic behaviour at about 118 min after injection time. This was carried out with surface approach speed of 0.6 nm s^{-1}. In the successive measurement within the same experiment at 162 min, with surface approach at 1.3 nm s^{-1}, we observed more structured layers, smaller surface separation at the innermost layer and longer decay lengths. The viscosity of 80 vol% EAN is about 6.3 mPa s.[33] From our previous studies, 1.3 nm s^{-1} is within the range where the viscous force is not significant for long-range decay.[30] This is also evidenced when we compare the force profiles at 235 min and 446 min which were measured at slow speeds of 0.8 nm s^{-1} and 0.6 nm s^{-1} showing very similar long-range decay.

Considering these observations together, it appears that the equilibration of the nearest surface layers of EAN can be very slow to evolve. This resonates with several previous reports of very slow dynamics of ionic liquids at interfaces,[34,35] and it may be that the EAN–water mixture forms self-assembled nanostructure on mica surfaces over time.[35]

VI.   Conclusion

We have presented direct measurements of the interaction force between atomically smooth mica crystalline surfaces across mixtures of the salt

ethylammonium nitrate, EAN, with water. EAN is a protic ionic liquid (protic molten salt) in its pure form, and is miscible with water in all volume fractions. Despite this, it is know that EAN and water retain their own nano-scale structural features in mixtures, due to nanostructuring and segregation in the bulk fluid.[29] Our measurements span the concentration range from 10 vol% EAN to 100 vol% EAN and have very high resolution in distance of about 0.1 nm and in interaction free energy of $\sim 10^{-5}$ J m^{-2}; the results reveal a range of features. At the highest EAN concentrations, surface interactions are characterised by oscillatory forces at short range (typically in the range $D < 5$ nm) and, beyond this, a monotonically decaying force of apparently exponential form measurable to about 15–20 nm. At lower EAN concentrations the short-range oscillations become less well defined and the decay length of the tail decreases. At 10 vol% EAN we observed only very short-range forces, and there was some variation between experiments. At concentrations $\geq$ 80 vol%, the short-ranged structure, when observed, had wavelength close to the average dimension of an EAN ion-pair and is interpreted as the 'structural force' or as arising from the co-ion correlations in the fluid as probed by the presence of interfaces. Interestingly, this short-range part of the force was dynamic and became sharper over the timescale of hours but not in the 100 vol% EAN; reminiscent of several previous studies with ionic liquids at interfaces.

The longest range part of the interaction, a monotonic tail with decay lengths in the range of 7 nm for the highest EAN concentrations, has been compared quantitatively to the scaling analysis previously considered for ionic liquids and salt solutions in water. The present results are consistent with the previously-observed scaling, and do not indicate any clear difference between protic and non-protic fluids.

A final comment is to note the interesting qualitative similarity in the form of interaction forces measured across electrolytes at extremely low and extremely high ion concentrations. Referring back to eqn (2), we see a possible rationalisation for this. In fluid condensed matter (liquids), there is always at least one component at high density and so always (at least) one mode giving rise to an oscillatory decaying term in the potential of mean force between particles or surfaces across the fluid. In dilute electrolytes, this is the solvent (e.g. water), giving rise to 'solvent (water) layering'; in highly concentrated electrolytes this is the salt and gives rise to 'salt layering' as seen here with 0.5 nm oscillations. In dilute electrolytes, the salt is at very low concentration and so gives rise to an additional plain exponential term arising from the ion–ion correlations, with decay parameter asymptotically tending towards the Debye length. In very concentrated electrolytes, the plain exponential decay with long decay length must arise from a contribution (eqn (2)) with low effective (renormalised) charge; fluctuating entities involving multiple associating (correlated) ions on the scale of the Bjerrum length.[2,12] This phenomenon appears in the present experiments with protic ionic liquids, just as in the earlier measurements with non-protic ILs and with simple salt solutions. The nature of charge and its distribution in dense electrolyte solutions remains of interest.

Conflicts of interest

There are no conflicts to declare.
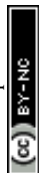
Acknowledgements

References

1 M. A. Gebbie, *et al.*, Ionic liquids behave as dilute electrolyte solutions, *Proc. Natl. Acad. Sci. U. S. A.*, 2013, **110**(24), 9674–9679.

2 M. A. Gebbie, *et al.*, Long-range electrostatic screening in ionic liquids, *Proc. Natl. Acad. Sci. U. S. A.*, 2015, **112**(24), 7432–7437.

3 A. M. Smith, A. A. Lee and S. Perkin, The electrostatic screening length in concentrated electrolytes increases with concentration, *J. Phys. Chem. Lett.*, 2016, **7**, 2157–2163.

4 R. M. Espinosa-Marzal, *et al.*, Ionic liquids confined in hydrophilic nanocontacts: Structure and lubricity in the presence of water, *J. Phys. Chem. C*, 2014, **118**, 6491–6503.

5 H.-W. Cheng, *et al.*, Characterizing the influence of water on charging and layering at electrified ionic-liquid/solid interfaces, *Adv. Mater. Interfaces*, 2015, **2**, 1500159.

6 N. Hjalmarsson, R. Atkin and M. W. Rutland, Switchable long-range double layer force observed in a protic ionic liquid, *Chem. Commun.*, 2017, **53**, 647–650.

7 P. Gaddam and W. Ducker, Electrostatic Screening Length in Concentrated Salt Solutions, *Langmuir*, 2019, **35**(17), 5719–5727.

8 B. V. Derjaguin, Friction and adhesion. IV. The theory of adhesion of small particles, *Kolloid-Z.*, 1934, **69**(2), 155–164.

9 J. E. Hallett, K. J. Agg and S. Perkin, Zwitterions fine-tune interactions in electrolyte solutions, *Proc. Natl. Acad. Sci. U. S. A.*, 2023, **120**, e2215585120.

10 D. F. Evans and H. Wennerström, *The colloidal domain : where physics, chemistry, biology, and technology meet*, Advances in Interfacial Engineering Series, Wiley-VCH, New York, Chichester, 2nd edn, 1999.

11 R. M. Pashley and J. N. Israelachvili, Molecular layering of water in thin films between mica surfaces and its relation to hydration forces, *J. Colloid Interface Sci.*, 1984, **101**(2), 511–523.

12 R. Kjellander, The intimate relationship between the dielectric response and the decay of intermolecular correlations and surface forces in electrolytes, *Soft Matter*, 2019, **15**(29), 5866–5895.

13 A. A. Lee, *et al.*, Scaling analysis of the screening length in concentrated electrolytes, *Phys. Rev. Lett.*, 2017, **119**, 026002.

14 A. A. Lee, *et al.*, Underscreening in concentrated electrolytes, *Faraday Discuss.*, 2017, **199**, 239–259.

15 S. Kumar, *et al.*, Absence of anomalous underscreening in highly concentrated aqueous electrolytes confined between smooth silica surfaces, *J. Colloid Interface Sci.*, 2022, **622**, 819–827.

16 B. Rotenberg, O. Bernard and J.-P. Hansen, Underscreening in ionic liquids: a first principles analysis, *J. Phys.: Condens. Matter*, 2018, **30**(5), 054005.

17 R. M. Adar, *et al.*, Screening length for finite-size ions in concentrated electrolytes, *Phys. Rev. E*, 2019, **100**(4), 042615.
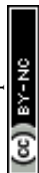
18 P. Cats, *et al.*, Primitive model electrolytes in the near and far field: Decay lengths from DFT and simulations, *J. Chem. Phys.*, 2021, **154**(12), 124504.

19 J. Zeman, S. Kondrat and C. Holm, Bulk ionic screening lengths from extremely large-scale molecular dynamics simulations, *Chem. Commun.*, 2020, **56**(100), 15635–15638.

20 N. B. Ludwig, *et al.*, Describing screening in dense ionic fluids with a charge-frustrated Ising model, *J. Chem. Phys.*, 2018, **149**(16), 164505.

21 J. Zwanikken and R. van Roij, Inflation of the screening length induced by Bjerrum pairs, *J. Phys.: Condens. Matter*, 2009, **21**(42), 424102.

22 A. Härtel, M. Bültmann and F. Coupette, Anomalous underscreening in the restricted primitive model, *Phys. Rev. Lett.*, 2023, **130**, 108202.

23 X. Zhang, *et al.*, Quantum mechanical effects in acid–base chemistry, *Chem. Sci.*, 2022, **13**(23), 6998–7006.

24 X.-Z. Li, B. Walker and A. Michaelides, Quantum nature of the hydrogen bond, *Proc. Natl. Acad. Sci. U. S. A.*, 2011, **108**(16), 6369–6373.

25 R. G. Horn, D. F. Evans and B. W. Ninham, Double-layerand solvation forces measured in a molten salt and its mixtures with water, *J. Phys. Chem.*, 1988, **92**(12), 3531–3537.

26 R. Atkin and G. G. Warr, Structure in confined room-temperature ionic liquids, *J. Phys. Chem. C*, 2007, **111**, 5162–5168.

27 R. Atkin and G. G. Warr, The Smallest Amphiphiles: Nanostructure in Protic Room-Temperature Ionic Liquids with Short Alkyl Groups, *J. Phys. Chem. B*, 2008, **112**(14), 4164–4166.

28 J. A. Smith, *et al.*, Surprising Particle Stability and Rapid Sedimentation Rates in an Ionic Liquid, *J. Phys. Chem. Lett.*, 2010, **1**(1), 64–68.

29 R. Hayes, *et al.*, How water dissolves in protic ionic liquids, *Angew. Chem., Int. Ed.*, 2012, **51**, 7468–7471.

30 R. Lhermerout and S. Perkin, Nanoconfined ionic liquids: disentangling electrostatic and viscous forces, *Phys. Rev. Fluids*, 2018, **3**, 014201.

31 J. N. Israelachvili, Thin film studies using multiple-beam interferometry, *J. Colloid Interface Sci.*, 1973, **44**(2), 259–272.

32 M. S. Azam, *et al.*, Silica Surface Charge Enhancement at Elevated Temperatures Revealed by Interfacial Water Signals, *J. Am. Chem. Soc.*, 2020, **142**(2), 669–673.

33 R. Zarrougui, M. Dhahbi and D. Lemordant, Transport and Thermodynamic Properties of Ethylammonium Nitrate–Water Binary Mixtures: Effect of Temperature and Composition, *J. Solution Chem.*, 2015, **44**(3), 686–702.

34 M. Han and R. M. Espinosa-Marzal, Electroviscous Retardation of the Squeeze Out of Nanoconfined Ionic Liquids, *J. Phys. Chem. C*, 2018, **122**(37), 21344–21355.

35 H. Li, *et al.*, Extremely slow dynamics of ionic liquid self-assembled nanostructures near a solid surface, *J. Colloid Interface Sci.*, 2023, **630**, 658–665.